



# Application of 3D-scanning for structural and geometric assessment of aerospace structures

Lina van Brügge<sup>1</sup> · Kaan M. Çetin<sup>1</sup> · Sebastian J. Koeberle<sup>1</sup> · Moritz Thiele<sup>1</sup> · Fabian Sturm<sup>1</sup> · Mirko Hornung<sup>1</sup>

Received: 6 January 2022 / Revised: 25 February 2023 / Accepted: 13 March 2023 / Published online: 3 April 2023  
© The Author(s) 2023

## Abstract

The geometric assessment of physical demonstrators are an integral part of several research projects conducted at the Chair of Aircraft Design at the Technical University of Munich. The projects range from several research UAVs, a sailplane morphing wing to propellers. There are different project objectives like the assessment of manufacturing deviations, design and function validation as well as reverse engineering of aerodynamic surfaces for model adaptation and simulation in the projects. Nevertheless, mutual approaches and solutions have been identified. Therefore joint development efforts are undertaken using 3D-scanning technology for data collection and evaluation. This technology captures the surface of a given object typically as a point cloud with comparably high accuracy. Since a manual evaluation process bears disadvantages in terms of reproducibility, custom post-processing software tools are developed. Global geometry data, like wing platform data, as well as airfoils can be extracted from a surface point cloud to analyze UAV wings or propellers. Airfoils can be derotated, normed and smoothed for aerodynamic analysis with low-fidelity aerodynamic tools, such as XFLR5 or XFOIL. For the analysis of morphing airfoil structures, the scanned geometry is aligned with the desired design airfoil shape so they can be compared. In this paper, analysis methods and several example results are presented.

**Keywords** Remotely piloted aircraft system (RPAS) · Unmanned aerial system (UAS) · Unmanned aerial vehicle (UAV) · 3D-scanning · Geometry extraction · Morphing wing structures · Polynomial smoothing · PCA · Reverse engineering

## 1 Introduction

With the maturation of 3D-scanning tools for recording surfaces and related methods for data evaluation, 3D-scanning has proliferated widely, both in terms of fields of application

as well as in scale of magnitude. While the applications typically share the initial recording and representation of surface data as the first process step, differences arise in the usage of data that can be loosely classified in three categories [1]:

- *Documentation*, e.g. of products for comparing actual shapes to desired shapes in the course of quality control.
- *Digitization*, e.g. of machine components for producing spare parts or retrofitting equipment to key interfaces such as threads or functional surfaces.
- *Reverse engineering*, e.g. extracting the characteristics of aerodynamic surfaces such as airfoil geometries or taper to reconstruct a design methodology.

While extensive and mature tools for documentation and digitization are available and applicable for a comparably large range of structures, tools for reverse engineering need to be tailored to the structure of interest to benefit from knowledge of domain-specific methods. In case of aerospace structures like wings, considering domain-specific knowledge is necessary to reverse engineer design geometries,

---

✉ Lina van Brügge  
lina@vanbruegge.de

Kaan M. Çetin  
kaanm.cetin@gmail.com

Sebastian J. Koeberle  
sebastian.koeberle@tum.de

Moritz Thiele  
moritz.thiele@tum.de

Fabian Sturm  
fabian.sturm@tum.de

Mirko Hornung  
mirko.hornung@tum.de

<sup>1</sup> Technical University of Munich, TUM School of Engineering and Design, Chair of Aircraft Design, Boltzmannstr. 15, Garching, Munich 85748, Germany

such as airfoils, that underlie the resulting geometries of wings and propellers. Furthermore, reverse engineering tools have to consider the intended usage of results such as analyzing aerodynamics, in which case resulting geometries have to meet requirements arising from the analysis tools employed downstream. In the following, several case studies are presented that exemplify challenges and aspects to consider when applying 3D-scanning for reverse engineering tasks to solve problems arising in research projects in the field of aerospace.

Several research projects of the Institute of Aircraft Design at the Technical University of Munich include the reverse engineering and assessment of physical technology demonstrators to validate and verify the methodologies developed [2]. Examples of such projects are the project *MILAN—Morphing Wings for Sailplanes* which is targeting an increase of lift-to-drag ratio and high-speed performance by implementing a wing featuring a deformable (morphing) forward airfoil section in combination with a hinged trailing edge flap [3, 4]. In the projects *FLEXOP* [5] and *FLiPASED* [6] the technology demonstrator *T-FLEX* is being utilized to demonstrate flutter mitigation and suppression as well as drag-reduction technologies in flight. Further projects target the prediction of flight dynamics characteristics of Unmanned Aerial Vehicles (UAVs) [7] themselves as well as the optimisation of propellers for UAVs [8] using physical specimen. Even though the aforementioned projects' nature and goals differ, mutual interests have been identified to employ 3D-scanning for capturing and assessing the geometry of physical specimen. Typically, 3D-scanning is utilized in pursuit of one of the following objectives:

1. Reverse engineering of design geometries for aerodynamic simulation purposes such as flight dynamics prediction and propeller assessment and optimization.
2. Assessment of geometric deviations of the physical structural part from the design shapes for validation of its function (*MILAN*) and model updates (*MILAN*, *FLEXOP*, *FLiPASED*).

In the first case, the ideal design geometries such as airfoils of aerodynamic surfaces are reconstructed from the 3D-scan data. Models using this data to predict the aerodynamic properties of the propeller or airframe can then be validated against test series that have been carried out. Here, it is possible to utilize additional knowledge of the design methodology to mitigate the influence of inaccurate or noisy 3D-scan data. In the second case, the accurate measurement of the actual geometry of the physical specimen is of interest, e.g. to update aerodynamic models in the project *FLEXOP* or *FLiPASED* to adjust predictions. Another use case is to assess if the actual deformations of the morphing airfoil section and wing bending match with the predictions in

the project *MILAN*. In terms of data evaluation, the second objective poses the additional difficulty to discern manufacturing deviation from inaccurate 3D-scan data.

In the assessment of 3D-scan data, the application of standard software suites has been found to bear disadvantages in terms of repeatability due to high reliance on manual user input. Furthermore, the 3D-scan data assessment does not account for possible a-priori knowledge in terms of design methodology for aerodynamic airfoils and extracted geometries which are typically not suited for usage in aerodynamic tools such as *XFOIL* [9]. Therefore, efforts are undertaken to develop a custom evaluation tool for 3D-scan data suited to meet the aforementioned objectives. Similar efforts have been undertaken by Gryte et al. [10] and Dantsker [11]. In the first publication, a 3D-scan of the Skywalker X8 was used to extract needed airfoils and the geometry for a reconstruction of the Remotely Piloted Aerial System (RPAS) in the low-fidelity simulation tool *XFLR5* [12]. Since the resolution of the scan was found to be insufficient for the analysis in *XFLR5*, the airfoils were manually smoothed and subsequently compared to the results of wind tunnel tests. In the second publication, Dantsker developed a custom *MATLAB* tool to extract airfoils of a 3D-scan. The airfoil was compared to the nominal airfoil and the deviations were explained by manufacturing inaccuracies which seems likely due to the construction method of the wing. The tool greatly reduces the need for manual input, however, the quality of the airfoil extraction approach has not been assessed in further detail.

Up to date, development efforts have been focused on the geometric characterization of aerodynamic surfaces of UAVs and propellers [13–15]. The extracted geometric characteristics, such as wing positions, airfoils and aerodynamic angles, proved suitable for usage in low-fidelity aerodynamic simulation. In the project *MILAN*, the deformations of the morphing airfoil section have been investigated, to assess the function of the compliant mechanism that is deforming the airfoil [16]. In the following chapters, the process of 3D-scanning and the method of geometry extraction are presented. Particular attention is given to the methods of data smoothing. The metrics of geometric and aerodynamic evaluation of results are introduced and the methodology is assessed using case studies on specimen of known geometry.

## 2 3D-scanning process and geometry extraction

### 2.1 Overview of the 3D-scanning process

The 3D-scanning and data extraction approach is composed of consecutive steps that are outlined in Fig. 1.

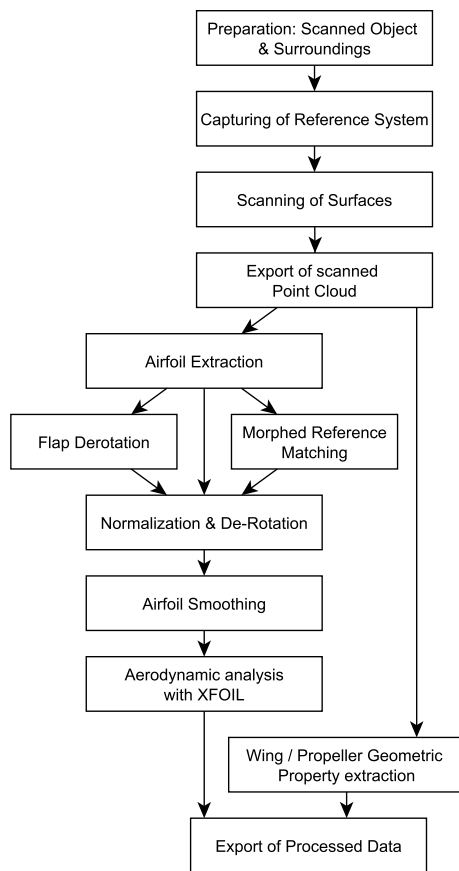


Fig. 1 3D-scanning toolchain

Several steps only apply for certain use cases that are described in detail below:

1. Preparation of the research object and the surroundings
2. Capturing of a reference system, using photogrammetry (*MaxSHOT 3D*) in case of large target objects
3. Scanning the relevant surfaces, using a laser 3D-scanner (*HandySCAN 700*) (also defines the reference system if photogrammetry is not used)
4. Exporting the scanned data as a point cloud
5. Post-processing using software tools
  - (a) Extraction of relevant cross-sections
  - (b) Flap derotation if necessary
  - (c) Matching of reference markers for morphed airfoils if necessary
  - (d) Normalization and derotation of the airfoil
  - (e) Airfoil Smoothing, if required
  - (f) Derivation of aircraft-level/propeller geometric properties such as dihedral, incidence angle a.o.



Fig. 2 Scan environment for large objects using the *MaxSHOT 3D* to capture the reference system [15]

## 2.2 Available hardware

A hand-held laser 3D-scanner of type *CREAFORM HandySCAN 700* [17] in combination with an optical coordinate measurement system (photogrammetric triangulation) of type *CREAFORM MaxSHOT 3D* [18] is utilized for the collection of surface data. The system utilizes a static coordinate system generated by circular target points that are applied either on the rigid object or surrounding surfaces. These points are captured by the coordinate measurement system with a photo camera from different angles. The 3D-scanner employs these points to determine its orientation in space and generates a surface point cloud with the help of reflecting laser beams. At least six points have to be in the field of view and in range (approx. 300 mm) of the 3D-scanner at a time for it to be able to orientate itself in space.

The volumetric accuracy of the coordinate measurement system *CREAFORM MaxSHOT 3D* is dependent on the size of the scanned object and is stated with 0.025 mm/m while the average deviation is 0.008 mm/m. The volumetric accuracy of the 3D-scanner *CREAFORM HandySCAN 3D* is 0.020 mm + 0.060 mm/m alone and 0.020 mm + 0.025 mm/m in combination with the coordinate measuring system *CREAFORM MaxSHOT 3D* with a resolution of 0.050 mm.

The coordinate measurement system *CREAFORM MaxSHOT 3D* is used for larger objects like UAVs or sailplane wing segments (MILAN: 500 mm chord length) to reduce the average deviation and increase the volumetric accuracy of the 3D-scanner.

## 2.3 Scan preparation

The scan process poses different challenges depending on the size and complexity of the scanned objects. In case of larger objects, target points can be applied on the aircraft surfaces, together with some targets outside the surfaces that are visible from multiple viewpoints as seen in Fig. 2. On

the other hand, placing enough targets on smaller objects like propellers proves difficult, which is why these objects require the construction of a suitable scanning environment or a background as shown in Fig. 3. This background must be sufficiently close to the object for the scanner to recognize the targets while ensuring accessibility to the scanned object from all sides. Ideally this background features targets visible from multiple viewpoints for the scanner to correctly align itself when scanning the sides of an object. Additionally, the surface of the object has to be matt to avoid unwanted reflections of the laser beams. However, matting spray hinders the proper application of target points when placed on the object itself.

## 2.4 3D-scanning process

The scanning process starts with the creation of a reference system where the targets are registered separately. The global reference targets are photographed using the *MaxSHOT 3D* for big objects as a first step. Standard scanning targets are captured directly by the *HandySCAN 700*. A specific part of the object is chosen as the origin of the coordinate system and the scan aligns accordingly. The scanning of the object can be started by scanning in a star-like fashion from the center to the outer edges of the object after the coordinate measurement system is resolved successfully. Challenges arise for the transition from the upper to the lower surface of thin surfaces such as wings or propellers via the leading or trailing edge. The placement of small tetrahedrons



**Fig. 3** Exemplary scan environment for a propeller with a diameter of 0.66m

fitted with scanning targets on the upper side of a wing helps this transition. The scanner provides the ability to merge multiple scan partitions from the same object if sufficient overlay of targets or surface geometry is present. This will, however introduce a further source of error as the merging process will lead to uncertainties at the edges. On sharp trailing edges, the system reaches its limits of resolution and accuracy. This problem arises not only on small scales, like propellers, but also in the scanning of the wing or tail of a UAV. This requires extra care and time when scanning these sharp edges and furthermore the extensive framework for post-processing that is described below. Scanning of a UAV in its entirety can lead to big amounts of data, therefore approaches for data reduction using lower resolutions are investigated. As a primary approach, a resolution of 0.5 mm [13] was used, which requires a high computational power. To reduce the number of points and reduce the time of computation, the resolution is reduced to 1 mm [15, 16] for objects with dimensions up to 6 m. Table 1 shows exemplarily the number of data points in a point cloud depending on the size of the scanned object.

A further application of the scanning process is the assessment of global wing deformations (bending, twist) measured on discrete points under load. This is achieved by defining specific recognizable reference points on the structure, and then scanning the object. Afterwards a predefined load is applied and the structure scanned again. The deformation can be evaluated by comparing the location of the reference points.

## 2.5 Post-processing and geometry extraction

The cleaning of the data and the removal of outliers is accomplished using the *CREAFORM VXmodel* tool. Also the merging of different scans is done in this environment. The data is exported as a point cloud consisting of 3D coordinates of the vertices on the scanned surface. These are then imported in the implemented tool. The geometry extraction

**Table 1** List of scanned object dimensions and corresponding point cloud sizes

Scanned object	Object size [mm/"]	Total number of point cloud points [Million]
Lizard Jet	Wingspan: 1380 Length: 1550	6.60
DG-800 S	Wingspan: 6000 Length: 2350	10.05
IMPULLS	Wingspan: 4993 Length: 2997	9.81
Morphing wing Demonstrator	Spanwise Length: 500 Profile Depth: 550	0.35
Tiger Propeller	Dimensions: 27 × 8.8	0.6



from the exported data is then accomplished in five general steps.

1. Orientation of the point cloud
2. Sectioning at predefined positions
3. Derotating of the deflected flaps, derotation of airfoils
4. Smoothing the airfoil shape, normalization of the airfoil geometry
5. Exporting airfoil and geometric characteristics

Some of these steps like the derotation of the flaps or the smoothing process of the airfoil are optional and have been implemented to deal with inaccuracies in the scan such as small defects due to false reflections. On the other hand, the orientation step is obligatory for all sections to define a conclusive, body-fixed coordinate frame.

**Orientation** For the orientation of the point cloud data different methodologies are used depending on the scanned object. The choice of method is taken by the user: If the scan object can present a reference axis (e.g. the attachment holes of a propeller) this axis can be used to determine the orientation of the point cloud in the *CREAFORM VXmodel* software. In case the object to be scanned does not provide a reference geometry (e.g. the scan of a complete aircraft) principal component analysis is used, in combination with assumptions about the aircraft investigated such as symmetry of the left and right side and minimal expansion in the z-axis. The main axes of the point cloud are determined by calculating the eigenvalues of the covariance matrix and the point cloud is oriented according to these calculated main axes. The direction of the largest dimension is aligned with the x-axis (typically spanwise), the second largest dimension aligned with the y-axis (typically in direction of the fuselage). The z-axis is finally aligned perpendicular to the x- and y-axes. It is important to mention, that this approach does not determine the final orientation of the point cloud, it will rather turn it in the right direction. It is possible that the point cloud of one 3D-scan is upside down while another scan is not. This depends on the exported coordinate system of the 3D-scan data and is solved in the implementation in the subsequent post-processing of the airfoil. An exemplary oriented bounding box can be seen in Fig. 4.

**Sectioning** The sectioning routine was introduced in [13] and further improved in [15]. The locations of the sections can be chosen in two different manners: Selection with a GUI via cursor click on the depicted parts of the object or with an input file to improve the accuracy. The first method uses a minimization of the thickness of the airfoil to determine the sectioning plane orthogonal to the wing. Firstly, a projection of all points within a defined, perpendicular distance  $d$  from the sectioning distance is conducted onto a plane. The sectioning distance is defined as a distance parallel to the x-axis of the coordinate frame. As the wings are

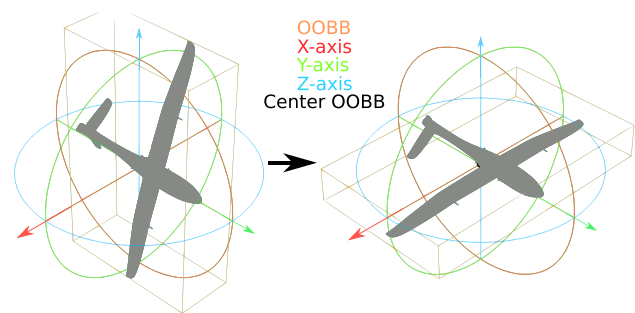


Fig. 4 Alignment of the UAV using a bounding box [15]

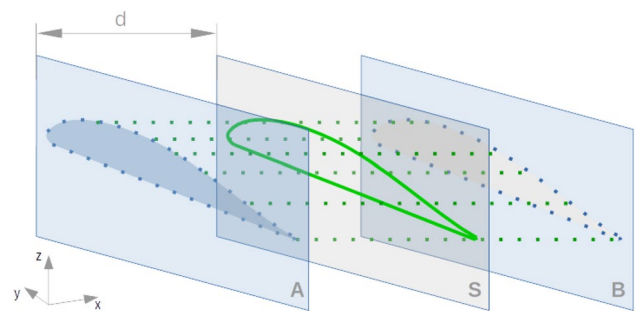


Fig. 5 Sectioning process of the point cloud using a sectioning plane  $S$  at defined location by projecting the points within the perpendicular distance  $d$  [13]

typically not parallel to the x-axis due to dihedral, the initial sectioning plane is not perpendicular to the wing. To find the section perpendicular to the wing and thus the airfoil, the plane is rotated until the minimum airfoil thickness is observed. This computation is achieved by a generic global optimization algorithm. The main working principle of the projection method algorithm is visualized in Fig. 5.

The second approach for the sectioning process of the wing and tail is based on the normal vectors of the point cloud surface. These normal vectors are computed beforehand with a Moving Least Square algorithm. The algorithm reconstructs a surface within a defined radius of a point and stores both, the normal vector and the point, in a new point cloud. This method is then executed for all points of the cloud. The normal vectors are prone to computational errors in addition to the defects of the 3D-scanning process. Therefore, all normal vectors at the chosen sectioning distance are averaged to gain a more accurate surface normal vector. The cutting plane can then be constructed using the computed surface normal vector and the unit vector in y-direction. With this method, it can be guaranteed that the lifting surface is sectioned orthogonal to the wing without multiple sectioning procedures at the same position. The airfoil is again generated via the projection of the nearest points onto the constructed plane as shown above in Fig 5.

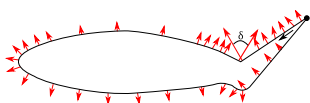


Fig. 6 Hinge line detection method [15]

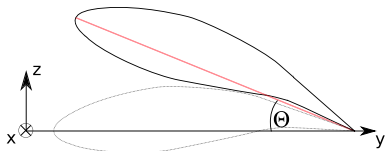


Fig. 7 Derotation of the airfoil about the incidence angle  $\Theta$  [15]

**Derotation of the Flaps and the Airfoil** During the scanning process it is possible that the control surfaces of the wing are not fixed at their exact neutral positions, which leads to inaccuracies in the airfoil continuity. Since it is difficult to determine the neutral position of flaps, i.e. the position in which the flaps align with the design airfoil, before scanning, the flaps are scanned in a deflected position and subsequently derotated numerically. It is important for this method to work, that the flaps are deflected in the direction of the hinge line. So, if the hinge line is on the upper side of the airfoil, the flaps have to be deflected upwards, on the lower side downwards. Since this method is only relevant for lifting surfaces containing a control surface, this routine is skipped when no flap is detected. The computation also utilizes the normal vectors of the sectioned airfoil. The algorithm searches for a discontinuity on the upper or lower half of the airfoil beginning at the trailing edge. The side of the airfoil which is chosen, is determined by deflection of the flaps and the position of the hinge line, respectively. If the flap is deflected upwards, the routine iterates the points on the upper surface of the airfoil and vice versa. The angles between the normal vectors of two adjacent points are computed. If the angle is greater than an appointed value, the point is stored as a candidate for the hinge line including the associated angle  $\delta$ . The foremost candidate is chosen as the hinge line. The stored angle is assigned as the derotation angle of the flap. The detection method is visualized in Fig. 6. For the derotation of the flap, the airfoil is split at the hinge line, the rear part of the airfoil is rotated by  $\delta$  and reassembled afterwards.

As soon as the continuous airfoil shape is reconstructed, the airfoil as a whole is derotated. For this, the rearmost and foremost points of the airfoil or rather the points with the maximum and minimum y-distance are selected. A vector between both points is computed and the airfoil is then rotated about the angle between the vector and the XY-plane which represents the incidence angle  $\Theta$  of the wing (see Fig. 7).

**Smoothing** After the derotation, the airfoil is smoothed, ordered and normalized. The main goal is to smooth out the errors, that arise during the scanning process. It may also be possible to smooth out the defects of the manufacturing process of the wing itself, but this was not investigated further. Without this additional smoothing operation, it is possible to compare the design airfoil to the scanned geometry. However, it is not possible to determine if the occurring deviations originated from the scanning or from the manufacturing process. The effect of different smoothing approaches have been examined in [15] and are presented in the result chapter. All post-processing steps could also be performed manually (see [10]), but have been automated to improve usability. The automated process follows these steps:

1. Computing the skeleton line of the airfoil
2. Splitting the airfoil in lower and upper side along the skeleton line
3. Ascendant ordering of the points in the upper/lower sides
4. Rearranging and up-sampling the points in a half using a spline
5. Smoothing using a polynomial interpolation
6. Down-sampling and concatenating both halves
7. Mirroring the airfoil at the x-/y-axis if needed
8. Normalizing, ordering and exporting

After the approximation of the skeleton line, the points of the airfoil are separated in points above and below the skeleton line. These points are still non-ordered, so they are arranged in an ascending manner of the x-values to form a valid spline input. Since cubic splines tend to oscillate if the points are not spaced equally, a Steffen spline [19] is used for the fitting. The points of the airfoil are upsampled and rearranged in a Chebyshev node distribution [20] to guarantee a stable polynomial fit. Equation 1 shows the distribution rule defined by Chebyshev.

$$x_k = \cos\left(\frac{2k-1}{2n}\pi\right), \quad k = 1, 2, \dots, n \quad (1)$$

Then, the polynomial can be used for the smoothing process of the curve. The influence of different polynomial degrees were examined in [15]. There, two different polynomial degrees were chosen depending on the maximum distance from the skeleton line of the curves. Therefore, the maximum and minimum y-values of the curves are compared. For curves with a small thickness, a polynomial of order 10 is fitted onto the curve and for curves with a greater thickness a polynomial of order 16 is used. Then, the upper and lower curves are reassembled afterwards. The last step before the normalization is to check the correct orientation of the airfoil. It is then mirrored at the y- or x-axis if necessary. The former is indicated by the curvature of the skeleton line. For

the latter, the vertical distance between two points on top and bottom surface near the trailing and the leading edge are computed and compared: The greater distance indicates the leading edge. Before the export in form of a DAT-file of data points, the airfoil is normalized and ordered counterclockwise from trailing edge to leading edge and back to trailing edge.

In addition to the airfoils, the dihedral and the incidence angle, the chord and the offset of the wing are computed and saved. The former is the difference between leading and trailing edge before the normalization and the latter is stored, using the  $y$ -value of the leading edge of each section.

**Morphing Wing** Another test-case where the 3D-scanning was utilized is the analysis of morphing wing geometries. For the analysis of demonstrator wing segments with a morphing forward section, a procedure has been developed. It has been implemented and tested by Kloiber [16]. In this case, neither the leading edge, nor the trailing edge is available as a geometric reference. The leading edge is moved due to elastic morphing and the hinged trailing edge flap is either deflected or left out to reduce the number of parts. Therefore two reference markings that are visible in the 3D-scan are applied on the rigid lower side of the wing. In the future those markings shall be created by CNC-milled recesses in the mold of the lower wing shell, so their positions are known exactly. The edges of those markings are identified in the scanned raw data of the airfoil cross-section via the step in the derivative of a function that is defined through the points. From these positions the scanned coordinates are moved, derotated and normalized with respect to the reference, design airfoil. The coordinate transformation method is sketched in Fig. 8.

If the trailing edge flap is missing, the coordinates in this area are taken from the reference airfoil. Also the coordinates of the two markings and those of the structural overlap are removed. Finally the completed and normalized airfoils can be analyzed geometrically and aerodynamically with *XFOIL 6.99* [9] to compare their performance with the designed airfoils.

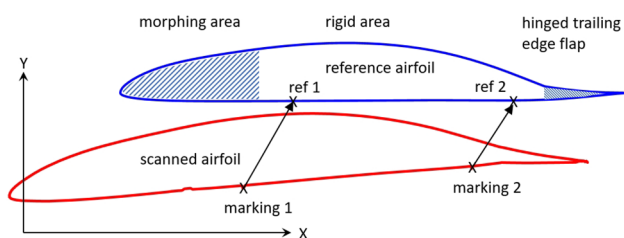


**Fig. 8** Coordinate transformation of scanned morphing airfoil with respect to reference airfoil [16]

### 3 Results

#### 3.1 Results of the tools

**Sectioning of wings** As an initial case study for the geometry extraction for reverse-engineering of the ideal design (i.e. objective 1 in Sect. 1), the wing of the UAV *Garfield* was chosen for its known airfoil data and the availability of a simple, rectangular relatively large wing section [13]. The UAV was sectioned with the minimization method and neither was the flap rotated nor the airfoil smoothed afterwards. A comparison of an extracted airfoil with the design airfoil are shown in Fig. 9.

It becomes apparent that the largest deviations between both airfoils can be found at the hinge line and the sealing. These two peaks show exemplary problems regarding the handling of the flaps and are the reason for the development of the flap derotation algorithm. The remaining deviations are comparable to the deviations stated by Selig et al. [21]. However, some peaks in the deviations is still present. All in all, wind tunnel accuracy as defined in [22, 23] could not be achieved and the origins for the deviations in general are mostly unclear. Possible candidates are manufacturing tolerances of the present rectangular wing section, tolerances of the 3D-scanner or errors within the sectioning tool. Subsequent work therefore focused on the reconstruction of airfoils featuring deflected flaps and the smoothing of the sectioned airfoil. An example of such a post-processed airfoil can be seen in Fig. 10. It was obtained from the research aircraft *IMPULLS*. In this plot, the largest deviation is still present at the hinge line. However, the airfoil now has a continuous surface which improves the results and convergence of further aerodynamic computations significantly.

**Sectioning of small objects** The smoothing algorithm is then tested on small-scale scanned data using the propeller “Madrono1”, again with the intention of reverse-engineering the ideal design (i.e. objective 1 in section 1). The propeller has been scanned, the airfoils extracted and smoothed.

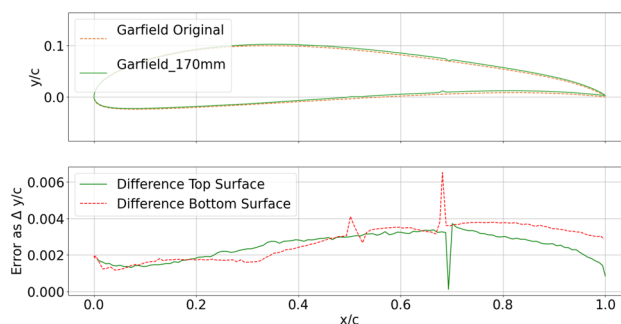


**Fig. 9** UAV *Garfield*: Total airfoil difference between the extracted airfoil (dashed line) at 170 mm and the original airfoil (solid line) [13]

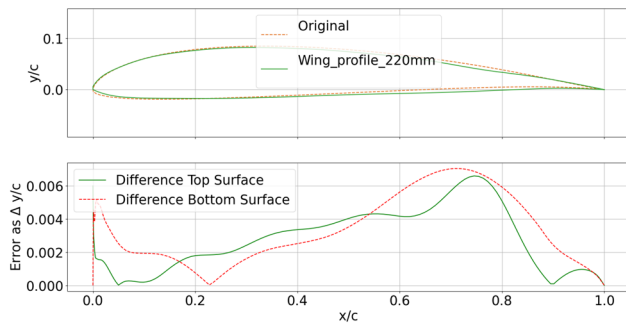


**Fig. 10** UAV *IMPULLS*: Total airfoil difference between the extracted airfoil (dashed line) at 220 mm and the original airfoil (solid line) [15]

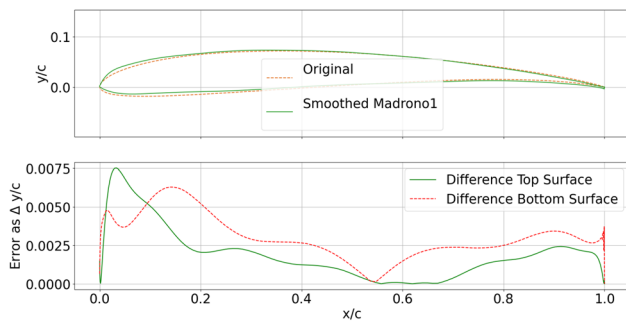


**Fig. 11** Madrono1 propeller: Comparison of extracted airfoil (dashed line) and design airfoil (solid line) in terms of geometric deviation

The propeller has a diameter of 63 cm and features a custom designed airfoil that is constant over the whole span. The extracted exemplary section has been chosen in the middle of the propeller at a radial position of 16.8 cm. The comparison of chord-wise, geometric error between the original airfoil and the smoothed algorithm output is depicted in Fig. 11.

The smoothing algorithm is able to produce a reconstructed airfoil that closely matches the original airfoil in the center part of the airfoil. However, the leading and trailing edge show increased deviations due to the geometric limits of the 3D-scan. The sharp leading and trailing edges of the propeller can not be represented accurately enough for the smoothing algorithm to receive adequate input data.

*Investigation of MILAN Morphing Wing Demonstrators*  
For the project *MILAN*, two small wing segment demonstrators with morphing forward sections have been built for the purpose of actual geometry assessment after deformation of the leading and trailing edge using 3D-scanning and the developed toolchain (i.e. objective 2 in Sect. 1). The wing sections both have a span-wise dimension of 500 mm and a chord length of 550 mm. The two demonstrators feature two different morphing shell structures.

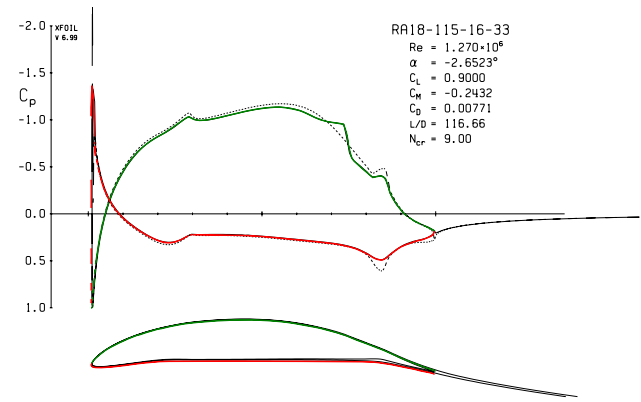


**Fig. 12** Pressure distribution of design airfoil in slow-flight configuration at  $c_l = 0.9$

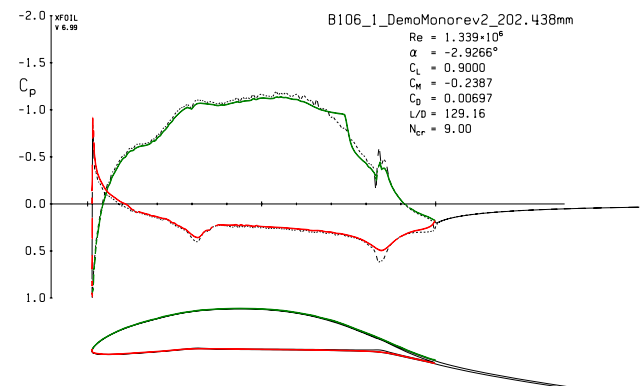


**Fig. 13** Pressure distribution of scanned geometry in slow-flight configuration at  $c_l = 0.9$  (monolithic shell demonstrator)

One employs a monolithic composite shell, the other one utilizes a shell of type *CellSkin* [4]. The objective is to analyze the resulting surface geometries both in fast-flight (nose and flap up) and slow-flight (nose and flap down) configuration and to compare the aerodynamic performances with the target airfoil shape performance. The pressure distribution of the design airfoil in slow-flight configuration at  $c_l = 0.9$  is shown in Fig. 12

In Fig. 13 the pressure distribution of the scanned geometry of one cross section in the monolithic demonstrator at  $c_l = 0.9$  is shown. Compared to the design airfoil in Fig. 12, the pressure distribution for the same lift coefficient shows a slightly different shape in the forward area, while the drag coefficient is kept almost the same. The inviscid pressure distribution shows a jagged shape, which is suspected to be caused by the point cloud processing. However, this has no significant effect on the position of the laminar-turbulent transition and the viscous drag in



this case. The effects of noisy scan data on aerodynamic simulation results have to be investigated further.

### 3.2 Validation of the tools

The toolchain has to be validated in the light of the existing results. The smoothing effect is visualized in Fig. 14 which shows the oscillations on the surface of the smoothed airfoil being reduced significantly. This is apparent in the lower graph of Fig. 14 where the error between the smoothed and the original airfoil is visible as a continuous line without unsteady spikes.

For the computation of the polars *XFLR5* v6.47 [12] was chosen (see Fig. 15). The lift coefficient of the smoothed airfoil matches the coefficient of the design airfoil rather well, while the original scan shows higher deviations.

estimated  $c_{l\ max}$  as well as the stall angle  $\alpha_{max}$  of the original scan is overestimated by 10%. The drag coefficient  $c_d$  is slightly overestimated for both the scanned and the smoothed airfoil for higher angles of attack, while the  $c_d$  of the smoothed airfoil matches the reference airfoil more closely for lower AoA.

As shown above, the smoothing process in general represents a good option to improve the results of the toolchain. To choose the best smoothing method, three different approaches were evaluated and compared to the design airfoil [15]. The airfoils are examined in terms of total geometrical difference to the design airfoil and by their polars. The different approaches cover the chosen polynomial fitting, a spline interpolation and a hybrid of polynomial and spline. This hybrid is also called “mixture” in Figs. 16 and 17 and is based on the assumption that the scan profile

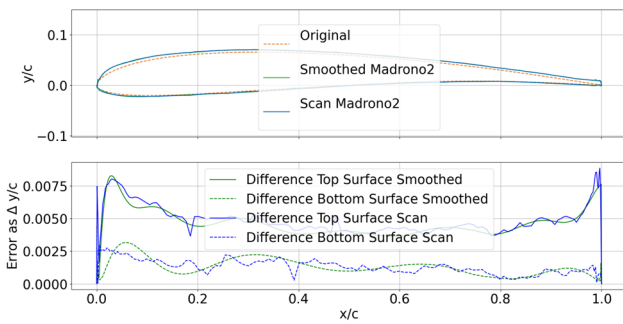


Fig. 14 Smoothing of defects and spikes by the smoothing algorithm on the propeller airfoil

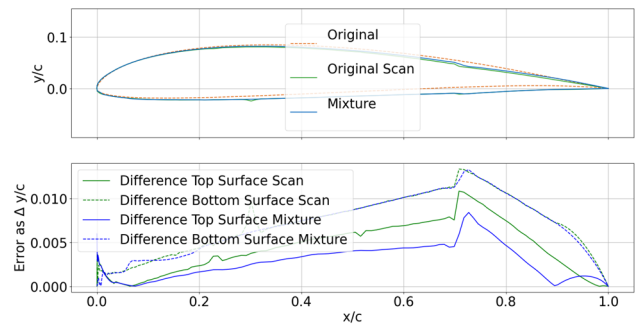
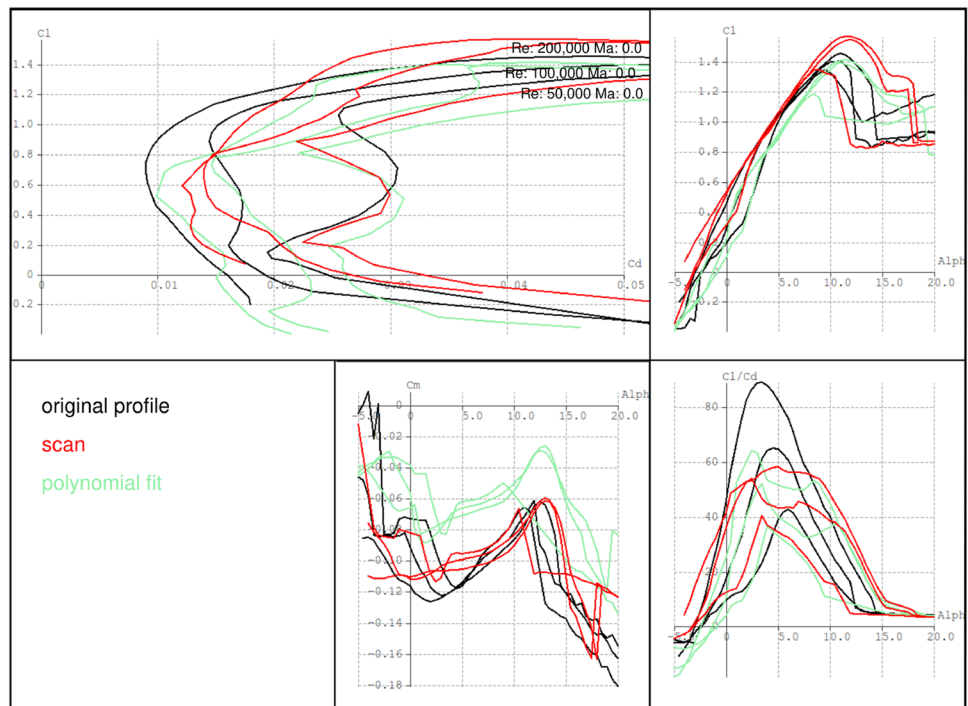
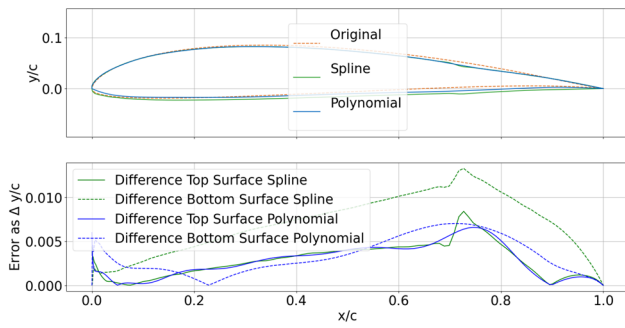


Fig. 16 Total airfoil difference between the extracted airfoil (hybrid and scan data) and the original profile [15]

Fig. 15 Exemplary polars of the 3D-scan, the smoothed airfoil and the original airfoil of the “Madrono1” propeller





**Fig. 17** Total airfoil difference between the extracted airfoil (spline and polynomial data) and the original profile [15]

approximates the original airfoil best but has a discontinuous surface which has to be smoothed first. The total difference of the airfoils compared to the design airfoil is shown in Figs. 16 and 17.

The largest total difference over all approaches is located at the hinge line. This can be explained by a non-complete derotation of the flap during the sectioning process. The average geometric difference of the airfoil on the other hand has been decreased with all of the approaches. While the scan features an average error of  $4.61 \cdot 10^{-3}$ , the hybrid shows only  $3.97 \cdot 10^{-3}$  of average error, the spline  $3.99 \cdot 10^{-3}$  and the polynomial even  $2.66 \cdot 10^{-3}$  which corresponds to two thirds of the scan difference. Additionally, every approach is able to smooth out the defects of the scanning process. This improves the convergence of the polar calculation significantly.

The results of the aerodynamic comparison resemble the observed geometric differences. The polars of the hybrid and the original scan data reach the lowest lift coefficient from all fitting methods (see Fig. 18). The computed coefficients of the spline and the polynomial approximate the original airfoil significantly better. The highest  $c_l$ -value was computed by the airfoil fitted to the spline. However, this value is above the maximum value of the original foil. In addition, the maximum of the  $c_{l\alpha}$  curve of the spline is shifted about several degrees of the AoA. In contrast to this, the maximum of the polynomial fit is almost at the same AoA as the one of the original airfoil. Overall, it should also be mentioned that the polar at low Reynolds numbers is represented very well with each smoothing method and without. (see Figs. 18 and 19).

Since the largest difference of the airfoil in comparison to the original airfoil occurs at the hinge line, no matter which post processing approach was chosen, a comparison between an airfoil with derotated flap and one without any flap is shown in Fig. 20. Both were smoothed with the presented polynomial fitting. The average error is even less than the one of the derotated flap and amounts to  $1.71 \cdot 10^{-3}$ . The bottom surface only has a small deviation of the original airfoil but displays minor oscillations. This is the result of a non-optimal polynomial order of the smoothing process. Future work could improve this problem by adding a greater variety of fitting degrees. Also, the top surface has a lower maximum deviation than the one with derotated flap. However, in the front part of the airfoil, the difference of the top surface of the airfoil with derotated flap is even less than the one

**Fig. 18** Comparison of the computed polars of the mixture and the scan data to the original airfoil

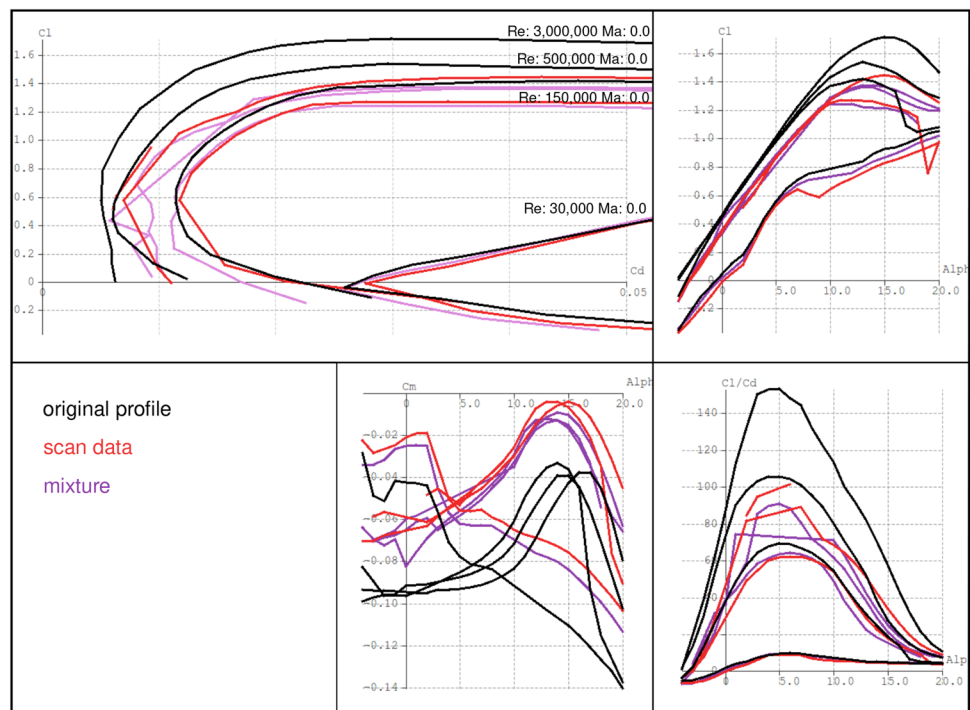


**Fig. 19** Comparison of the computed polars of the spline and the polynomial to the original airfoil

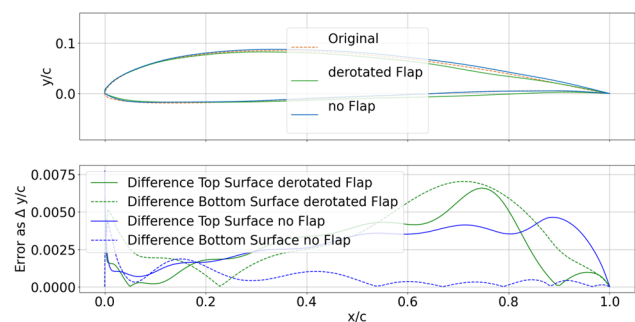
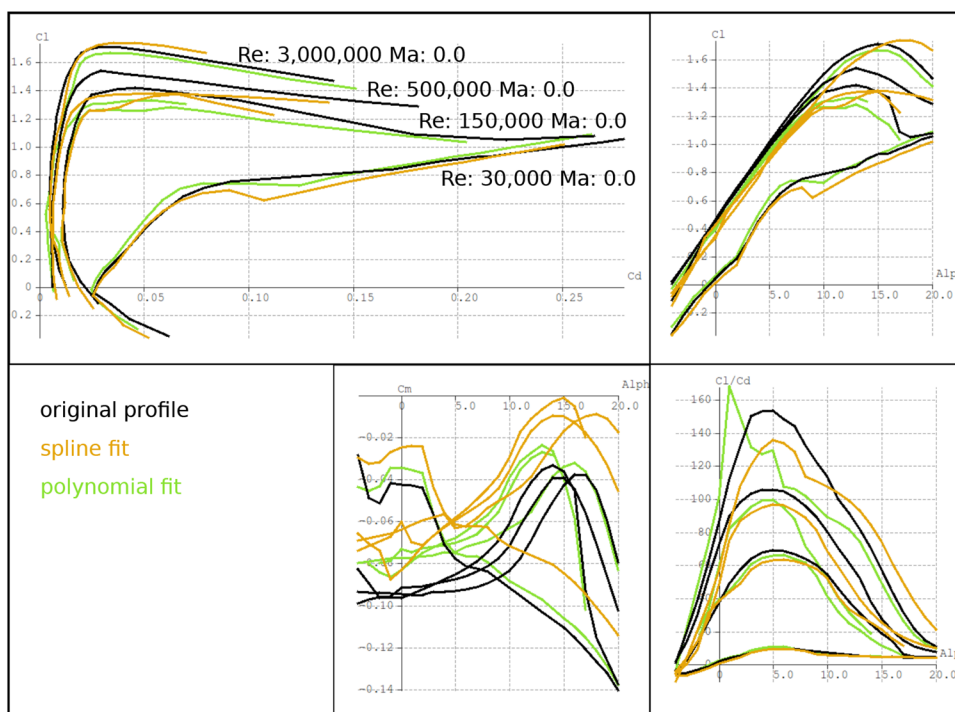


**Fig. 20** Difference between an airfoil with a derotated flap and one without any flap compared to the design airfoil

without. This difference was not evaluated further, but it is possible that it originates from the location of the second airfoil at the wingtip in combination with a large resolution of the 3D-scan which was chosen to reduce the amount of data present in the point cloud. This can also be the reason that the computed polars of the second airfoil were significantly worse than the one with the derotated flap. The resolution defect was examined by Busch [14] with respect to small propeller geometries.

### 4 Summary

The presented toolchain is capable of extracting and examining lifting surfaces of various aerospace applications and their characteristics. In this context, it is very important to

differentiate between geometrical and aerodynamic differences since not every geometrical difference implies a similar aerodynamic effect and vice versa. There is also a significant difference between Reverse Engineering and geometrical assessment. In the former, the reconstruction of the design intention is the main objective. This is mostly part of the propeller research. In contrast, the project MILAN is concentrating on the latter to obtain information of how the method of construction affects the aerodynamic behavior. All in all, 3D-scan is a powerful and useful tool to gain surface information. It is possible to obtain plausible results, but this can be a long way to go. Weaknesses are for example defects in the scanning process or the interaction between the point cloud and the implemented tools.

### 5 Outlook

Future work will primarily focus on assessing the geometric deviations between CAD-data and manufactured geometries in order to identify the origin of aforementioned geometric deviations, the characteristics of different smoothing algorithms and their actual impact on the results of aerodynamic simulations: To gain a deeper understanding of differentiating between deviations introduced by manufacturing errors, deviations introduced by the 3D-scanning process and deviations introduced by smoothing algorithms, a follow up project will use point clouds of an UAV obtained using different models of 3D-scanners. Furthermore, the point clouds will be used for comparing the suitability of the presented

smoothing approach of fitting an ordinary polynomial with an approach of fitting a Bernstein polynomial, which offers more parameters for optimization and promises to describe especially the nose section of the profile more closely, thus improving the results obtained from aerodynamic simulations. Lastly, the effect of the geometrical deviations as well as smoothing algorithms on the results of aerodynamic simulations in terms of pressure distribution, laminar-turbulent transition and resulting aerodynamic coefficients will be investigated on the morphing wing demonstrator. For applications in Reverse Engineering, future work will focus on integrating available a priori knowledge, such as design guidelines, into the *Airfoil Extraction* step described to improve results. In this regard, work has to commence with researching relevant design heuristics and suitable ways of introducing it into the *Airfoil Extraction* step.

**Funding** Open Access funding enabled and organized by Projekt DEAL. Funding by Technical University of Munich. The project MILAN, Morphing wings for sailplanes, has been funded by the German Federal Ministry for Economic Affairs and Climate Action under the grant of the German Federal Aviation Research Program (Luftfahrtforschungsprogramm, LuFo) V-3.

**Code availability** Code available on github [24].

## Declarations

**Conflict of interest** The authors declare that they have no conflict of interest.

**Open Access** This article is licensed under a Creative Commons Attribution 4.0 International License, which permits use, sharing, adaptation, distribution and reproduction in any medium or format, as long as you give appropriate credit to the original author(s) and the source, provide a link to the Creative Commons licence, and indicate if changes were made. The images or other third party material in this article are included in the article's Creative Commons licence, unless indicated otherwise in a credit line to the material. If material is not included in the article's Creative Commons licence and your intended use is not permitted by statutory regulation or exceeds the permitted use, you will need to obtain permission directly from the copyright holder. To view a copy of this licence, visit <http://creativecommons.org/licenses/by/4.0/>.

## References

1. Javaid, M., Haleem, A., Pratap Singh, R., Suman, R.: Industrial perspectives of 3d scanning: features, roles and it's analytical applications. *Sens Int* **2**, 100114 (2021). <https://doi.org/10.1016/j.sintl.2021.100114>
2. Current research projects (15.03.2021). <https://www.lrg.tum.de/en/lls/research/current-projects/>
3. Achleitner, J., Rohde-Brandenburger, K., Rogalla von Bieberstein, P., Sturm, F., Hornung, M.: Aerodynamic design of a morphing wing sailplane, in *AIAA Aviation: Forum* (American Institute of Aeronautics and Astronautics, Reston, Virginia **2019**, 4 (2019). <https://doi.org/10.2514/6.2019-2816>
4. Sturm, F., Achleitner, J., Jocham, K., Hornung, M.: Studies of anisotropic wing shell concepts for a sailplane with a morphing forward wing section, in *AIAA Aviation: Forum* (American Institute of Aeronautics and Astronautics, Reston, Virginia **2019**, 4 (2019). <https://doi.org/10.2514/6.2019-2817>
5. Flexop (2015). <https://flexop.eu/>
6. Flight phase adaptive aero-servo-elastic aircraft design methods (2015). <https://cordis.europa.eu/project/id/815058>
7. Koeberle, S.J., Albert, A.E., Nagel, L.H., Hornung, M.: Flight testing for flight dynamics estimation of medium-sized uavs., in *AIAA Scitech 2021 Forum* (American Institute of Aeronautics and Astronautics, 2021). <https://doi.org/10.2514/6.2021-1526>
8. Thiele, M., Staudenmaier, A., Madabhushi Venkata, S., Hornung, M.: Development of a reinforcement learning inspired monte carlo tree search design optimization algorithm for fixed-wing vtol uav propellers, in *AIAA Scitech Forum 2020*. American Institute of Aeronautics and Astronautics, Reston (2020)
9. Drela, M., Youngren, H.: (4.3.2017). <https://web.mit.edu/drela/Public/web/xfoil/>
10. Gryte, K., Hann, R., Alam, M., Rohac, J., Johansen, T.A., Fossen, T.I.: Aerodynamic modeling of the skywalker x8 fixed-wing unmanned aerial vehicle, in 2018 International Conference on Unmanned Aircraft Systems (Institute of Electrical and Electronics Engineers, Piscataway, NJ, USA, 2018), pp. 826–835. <https://doi.org/10.1109/ICUAS.2018.8453370>
11. Dantsker, O.D.: Determining aerodynamic characteristics of an unmanned aerial vehicle using a 3d scanning technique, in 53rd AIAA Aerospace Sciences Meeting (American Institute of Aeronautics and Astronautics, Reston, Virginia, 01052015). <https://doi.org/10.2514/6.2015-0026>
12. XFLR5 (9.3.2020). <http://www.xflr5.tech/xflr5.htm>
13. Çetin, K.M.: Development and Implementation of a 3D-Scanning-Toolchain for the Characterization of UAVs. Bachelor's thesis, Technical University Munich (2020)
14. Busch, S.: Entwicklung einer reverse-engineering toolchain für uav propeller. Bachelors thesis, Technical University of Munich, München (2020)
15. van Brügge, L.: Development and Implementation of a 3D-Scanning-Toolchain for the Geometric Characterization of UAVs. Bachelor's thesis, Technical University Munich (2020)
16. Kloiber, F.: Geometrieanalyse von Flügelsegmenten mit formvariabler Vordersektion für ein Hochleistungssegelflugzeug mittels 3D-Laserscan und Photogrammetrie. Semester thesis, Technical University Munich (2021)
17. Der 3D-Scanner HandySCAN 3D (Creaform 3d, Lévis, Kanada, 2020). <https://www.creaform3d.com/de/messtechnik/tragbare-3d-scanner-handyscan-3d/technische-daten>
18. Optical coordinate measuring system: Maxshot 3d (Creaform 3d, Lévis, Kanada, 2021). <https://www.creaform3d.com/en/metrology-solutions/optical-measuring-systems-maxshot-3d>
19. Steffen, M.: A simple method for monotonic interpolation in one dimension., *Astronomy and Astrophysics* **239**, 443 (1990). <https://ui.adsabs.harvard.edu/abs/1990A&A...239..443S>



20. Stewart, G.W.: *Afternotes on Numerical Analysis* (Society for Industrial and Applied Mathematics, 1996)
21. Selig, M.S., Guglielmo, J.J., Broeren, A.P., Giguère, P.: *Summary of low-speed airfoil data, vol. 1*. SolarTech Publications, Virginia Beach (1995)
22. Masters, D.A., Taylor, N.J., Rendall, T.C.S., Allen, C.B., Poole, D.J.: Geometric comparison of aerofoil shape parameterization methods. *Am. Inst. Aeronaut. Astronaut.* **55**, 1575–1589 (2017). <https://doi.org/10.2514/1.J054943>
23. Kulfan, B.M., Bussoletti, J.E.: “fundamental” parametric geometry representations for aircraft component shapes, in 11th AIAA/ISSMO Multidisciplinary Analysis and Optimization Conference (American Institute of Aeronautics and Astronautics, Portsmouth, Virginia (2006). <https://doi.org/10.2514/6.2006-6948>
24. Pointcloudextractor (2022). <https://github.com/vBruegge/PointCloudExtractor>

**Publisher's Note** Springer Nature remains neutral with regard to jurisdictional claims in published maps and institutional affiliations.